Multiferroics

The interplay between ferroelectricity and magnetic order.

Master Thesis of **Anne Helena Arkenbout**

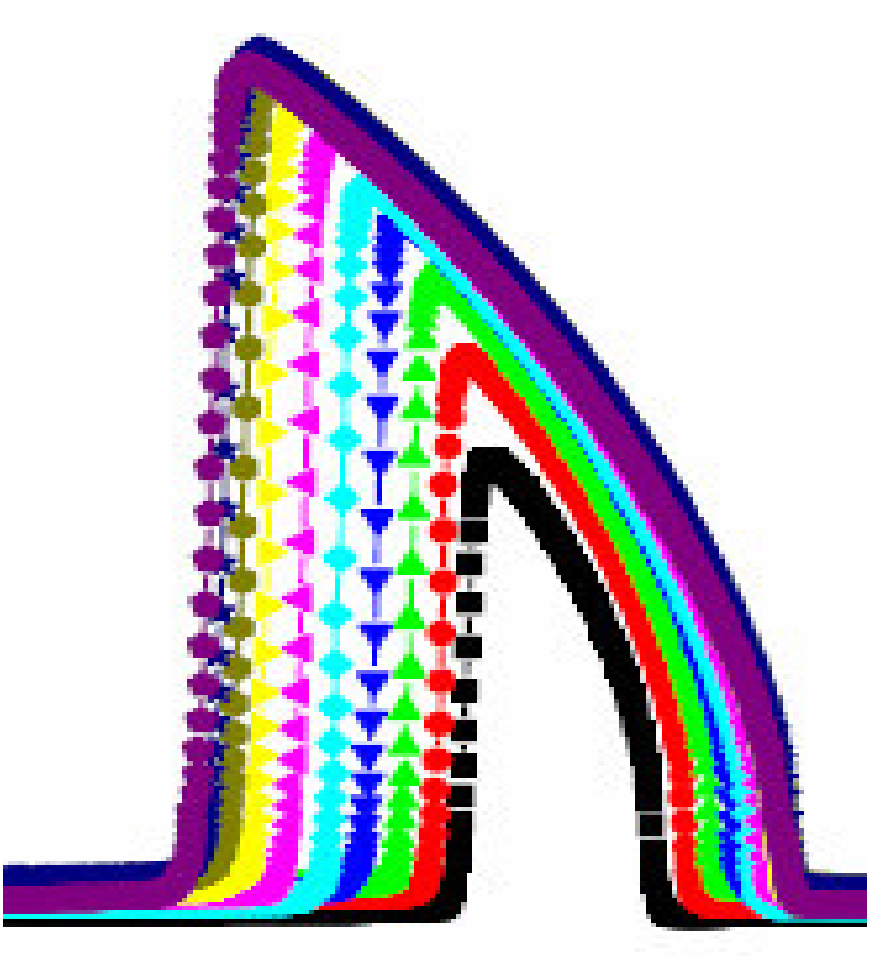

Supervised by: **T.T.M Palstra**
T. Kimura
G.R. Blake

Preface

This paper presents an overview of the work I did during the last year of my Nanoscience Top Master. This last year was almost completely devoted to research. The first six months of the research I worked on FeS in the Solid State Chemistry group prof. dr. T.T.M Palstra at the Material Science Center at the Rijksuniversiteit Groningen. This work was supervised by T.T.M. Palstra and Graeme Blake. The second part of this master thesis deals with my research on the multiferroic $MnWO_4$, which was performed during my three-month internship at Bell Laboratories, Lucent Technologies in Murray Hill, NJ (USA). This internship was supervised by A.P. Ramirez and T. Kimura.

Abstract

This report will present the research on two materials, FeS and $MnWO_4$, which are good candidates to show multiferroicity. Because FeS is a material that was suggested to show multiferroicity in several old publications, the first part of the research was focused on the determination of the physical properties of FeS. The x-ray diffraction and heat capacity measurements show a clear transition around 400 K, the temperature at which the ferroelectric phase transition was reported by van den Berg et al.[8] At this alpha transition a sudden change in the lattice parameters was observed. Moreover an anomaly could be observed in the electrical resistivity. However the conductivity in the material was to0 high to pole the sample and thus no pyroelectric measurements could be done. Therefore the question whether FeS is a possible candidate for ferroelectricity at room temperature remains unanswered.

The second part of the research was focused on the characterization of $MnWO_4$. In $MnWO_4$ single crystals the magnetic interactions are frustrated, such that three different magnetic structures are present below 13.5 K. Between 8 and 12.5 K the magnetic structure consists of a helical incommensurate spin density wave. Recent theories on ferroelectricity induced by magnetic ordering predict that such a spiral magnetic ordering will result in an electrical polarization. Dielectric and pyroelectric measurements show that the onset of the magnetic spiral structure in $MnWO_4$ is accompanied by the introduction of a polarization perpendicular to the spin rotation axis and the wave vector. These measurements are proof that the spiral magnetic phase of $MnWO_4$ is indeed multiferroic. As the amount of materials that show these properties is small, the discovery of ferroelectricity due to magnetic ordering in $MnWO_4$ will play an important role in the further development of the theory of the interactions in this type of materials.

Contents

Chapter 1: Introduction

Nowadays, industry is continuously looking for ways to improve the efficiency of computers. One of the important issues is the production of data storage media (like hard drives) with a higher data density, so that computers can work faster and take less space. From this perspective the current developments in the field of multiferroics might be very interesting. In general, a multiferroic is a material that possesses at least two of the following properties: ferroelectricity, magnetic ordering or ferroelasticity. Currently either ferroelectric or ferromagnetic materials are used for data storage media. If instead a multiferroic (with both magnetic and ferroelectric ordering) could be used as a memory, it would add an extra dimension to the field of data storage resulting in an increase of the data density.

Nevertheless, multiferroics are more than just materials that show a combination of ferroelectricity, magnetic order and ferroelasticity, they can in addition display a coupling between these properties. The coupling between electric and magnetic ordering is called the magnetoelectric effect and is defined as the induction of magnetization by an electric field or the induction of polarization by a magnetic field. Both the magnetoelectric effect and multiferroics themselves were already studied intensively in the 1960s, but as the results of this research were rather disappointing, the subject became less popular. The field has gained interest in the last five years, because recent developments in the theoretical background predicts that the magnetoelectric effect should be seen in a much wider range of materials than was concluded from the earlier publications.

The main reason for the disappointment in the sixties was the observation that, for the transition metal perovskites, ferroelectricity and magnetic ordering usually exclude each other. Namely, to observe any magnetic ordering, a transition metal should have unpaired d-electrons[1]. However, ferroelectricity was initially only observed for materials with the d^0 configuration. So it seemed that the magnetic order and the ferroelectricity could not coexist in one material. It was tried to introduce both d^0 and magnetic ions into one material to induce the combination of ferroelectricity and magnetism. An example of such a multiferroic is $BiFeO_3$, in which the Fe atoms are responsible for the magnetic order and the Bi atoms induce the ferroelectricity. Although these types of materials indeed show a combination of ferroelectricity and magnetic order, the magnetoelectric coupling in these materials is very small, because different atoms are at the origin of the magnetic and ferroelectric ordering. Thus the coexistence of magnetic ordering and ferroelectricity in combination with a strong magnetoelectric effect seemed impossible in this type of materials.

However, in 2003 Kimura et al.[2] showed that for the perovskite $TbMnO_3$ ferroelectricity and magnetic ordering do coexist at certain temperatures. The magnetic ordering in $TbMnO_3$ is a wavelike incommensurate structure with a wave vector (Q) of (0, 0.28, 1). At the transition temperature of this magnetic structure (30K) a sharp peak in the dielectric constant and the onset of a pyroelectric current could be observed, which are both features of a ferroelectric. As the ferroelectric phase transition occurred exactly at the same temperature as the magnetic transition it was suggested that the magnetic ordering induced the ferroelectricity. The very strong magnetoelectric and magneto capacitance effects that were present in this material supported this idea. In recent years

more materials were discovered that showed this magnetically induced ferroelectricity, like $TbMn_2O_5$ [3], $RMnO_3$ [4] (R=Gd and Dy) and $Ni_3V_2O_8$ [5].
This paper will be focused on two different materials FeS and $MnWO_4$. FeS is a hexagonal material consisting of Fe^{2+} ions that are surrounded by a distorted octahedron of sulfur atoms. It is very different in composition from the known multiferroics and the antiferromagnetic structure of FeS is not known to be spiral and induce the ferroelectricity as described in the theory of Mostovoy [6]. However, a famous review paper by Smolenskii [7] mentioned that this material might be a multiferroic. FeS is known to be an antiferromagnet with a Néel temperature around 600K. Van den Berg et al.[8] reported to have measured a pyroelectric current around 400 K, from which they concluded that the material is ferroelectric. Moreover, this transition seems to coincide with a magnetic phase transition in which the easy axis of the antiferromagnetic spins flip into another direction. On the basis of this information, FeS might be a multiferroic at room temperature. The statement by van den Berg, however was very controversial. Moreover, little is known about the possibility of multiferroicity in sulfides up to now. In chapter 3 an investigation focused on the properties on FeS and the question of whether it could be a multiferroic or not, will be presented.
The research on $MnWO_4$, presented in chapter 4, was motivated in a very different way. The magnetic structure of $MnWO_4$ is known to be frustrated below the Néel temperature of 13.5 K. This frustration leads to the appearance of several uncommon magnetic structures. At low temperatures the structure is an antiferromagnet with an up-up-down–down structure along the a axis. Above 8 K the magnetic ordering converts into a long-period helical spin density wave. At 12.5 K the spiral structure goes over into a sinusoidal wave [9]. According to the theory described by Mostovoy [6], a spiral magnetic structure should give rise to a polarization perpendicular to the incommensurate wave vector and the spin rotation axis. The research presented in chapter 4 is focused on the electric and magnetic properties of $MnWO_4$, which could provide the answer whether $MnWO_4$ is multiferroic or not.
This report will present research on two materials, FeS and $MnWO_4$, that are good candidates to show multiferroicity. The next chapter will give a short introduction on the theory behind different types of multiferroics. In the third chapter the research on FeS will be discussed. The fourth chapter will be focused on the electric and magnetic properties of $MnWO_4$. Finally, in the last chapter future prospects will be given on the different types of multiferroics. It will be discussed which type of multiferroic is the most promising and which obstacles need to be addressed before multiferroics can be implemented in devices.

Chapter 2: Background

Many different routes exist for combining ferroelectricity and magnetic order in one material[1,10]. However, the total number of known multiferroics is not very large because there are some fundamental contradictions in the conditions that are needed for magnetic ordering and ferroelectricity. In this chapter a short overview will be given on the most important types of multiferroics and their magnetoelectric coupling. Besides, a more extensive discussion will be given on the recently discovered class of multiferroics in which the ferroelectricity is induced by the magnetic order.

As already mentioned in chapter one, the transition metal d-electrons, which are essential for magnetism, reduce the tendency for off center ferroelectric distortion in perovskites. This empty d-orbital, apparently, is crucial for the observation of ferroelectricity[2]. The empty d orbital contributes in the bonding of the transition metal ion with one of the oxygen ligands because the interaction between the filled p-orbital of the oxygen atom and the empty d-orbital leads to a lowering of the energy, as is shown in figure 1. This bonding interaction results in an effective displacement of the transition metal towards the oxygen. When these displacements order over the whole crystal lattice, a net polarization can be obtained, resulting in ferroelectricity. If the d orbital contains an electron the overlap of the p-orbital on the oxygen and the d-orbital on the transition metal will not result in a reduction of the energy. Namely, the electron from the d-orbital would go into the anti-bonding orbital opposing the energy gain due to the electrons in the bonding state. Therefore, the bond between the transition metal and the oxygen will be less energetically favorable and the displacement, which is essential for ferroelectricity, does not occur.

To overcome this systematic exclusion attempts were made to incorporate magnetic cations in ferroelectric materials[11]. This method was successful in the formation of materials that showed both magnetic ordering and ferroelectricity, as for example $Pb_2(CoW)O_6$.

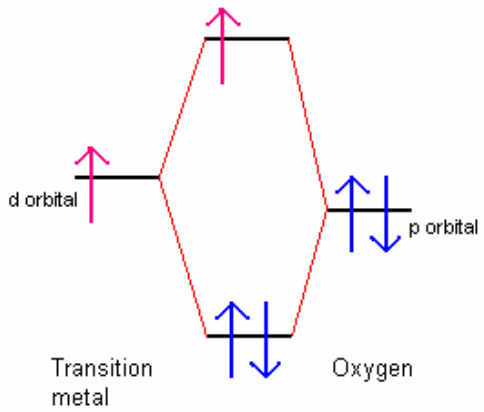

Figure 1: The d orbital of the transition metal forms a bond with the filled p-orbital of the oxygen ion. Both the oxygen electrons (arrows in blue) go into the bonding state. If electrons would be present in the d orbital of the transition metal (arrow in red), these electrons would fill up the anti-bonding orbital and weaken the bond between the transition metal and the oxygen.

However, due to the fact that the ferroelectricity and magnetic ordering have their origin in different atoms, the magnetoelectric effect was very small. Moreover, due to the dilution of the magnetic ions, the materials have a rather low Curie or Néel temperature.
Another group of materials that can get around this d^0 problem are those in which lone pair ions cause the ferroelectricity. An example of this type of multiferroics is $BiFeO_3$, in which the Bi^{3+} ion has a lone pair. Lone pairs are clouds of two electrons that are not bound to any other atoms. These lone pairs induce a strong local polarization that can result in ferroelectricity when the lone pairs on different atoms are correlated. The electrons on the other crystallographic site, Fe^{3+} (d^5), order independently from these lone pair ions to form a magnetic structure. So, just as in mixed multiferroics, these materials show weak coupling between the ferroelectric and magnetic order. However the transition temperatures can be very high: $BiFeO_3$ has a magnetic ordering temperature of 643 K and a ferroelectric ordering temperature of 1100K.
Another class of multiferroics is the hexagonal manganites. These materials have the same chemical formula as the perovskites ($AMnO_3$) in which A is a rare earth ion or yttrium. The crystallographic structure, however, is very different from the perovskites. The Mn^{3+} ions in theses hexagonal manganites are surrounded by a triangular bipyramid of oxygen atoms instead of an octahedron, and thus the electronic levels are very different. In this system the magnetic ordering normally sets in around 75K. The ferroelectricity is not caused by the Mn^{3+} ion but by the rare earth ion which is surrounded by 7 oxygen atoms[12]. The displacement of this rare earth ion is correlated with the tendency of the crystal structure to achieve close packing. This close packing induces the loss of inversion symmetry and thereby it creates a dipole on the A-O bond and when these dipoles order they induce a strong polarization. The ferroelectric phase transitions are therefore quite high; around 1000K.
The $BaMF_4$ are the only class of multiferroics known up till now that do not contain oxygen atoms. These materials crystallize in an orthorhombic structure and show piezoelectricity at room temperature[13]. The ferroelectric phase transition occurs at very high temperatures, around 1200-1500 K. The magnetic ordering sets in at much lower temperatures, namely around 70K[7].
As already mentioned in the introduction, recently another group of multiferroics was discovered: multiferroics in which the ferroelectricity is induced by magnetic order. For all these materials, the key factor in this magnetically induced ferroelectricity lies in the presence of spiral magnetic order[6]. The general relation between the polarization (P) and the magnetization (M) can be deduced from symmetry considerations. For cubic symmetry this relation is:

$$P = \gamma\chi_e [(M*\nabla)) M - M (\nabla*M)] \qquad (1)$$

were γ is the coupling constant and χ_e is the dielectric susceptibility. The magnetization for a spin density wave can be expressed as follows:

$$M = M_1 e_1 \cos Q*x + M_2 e_2 \sin Q*x + M_3 e_3 \qquad (2)$$

In this equation Q is the wave vector and the e_i are the unit vectors of which the e_3 axis is the spin rotation axis. If M_1 or M_2 is zero the magnetic structure describes a sine wave, if

they are both nonzero the wave is helical. From equation (1) and (2) it can be found that the average polarization (P') is given by equation (3).

$$P' = \gamma\chi_e M_1 M_2 [e_3 \times Q] \qquad (3)$$

As can be deduced from equation (3) as well as from the sketch in figure 2 the helical wave gives rise to an average polarization perpendicular to the wave vector Q and the spin rotation axis e_3. The sinusoidal wave does not induce an average polarization, because the inversion symmetry for this spin density wave remains unbroken.
It has been suggested that the Dzyaloshinskii-Moriya interaction is at the basis of this strong interaction between ferroelectricity and incommensurate magnetism[14]. The Dzyaloshinskii-Moriya interaction[15,16] (DMI) can stabilize a weak ferromagnetism in non-centrosymmetric antiferromagnetic materials due to spin orbit coupling and superexchange interactions. In a similar way this DMI is able to stabilize a spiral magnetic structure. The spiral in turn gives rise to a pattern of atomic displacements. These atomic displacements are crucial for the ferroelectricity but can be as small as $1*10^{-3}$Å and thus are very hard to determine experimentally. The results of the calculation of Sergienko[14] showed that the DMI will contribute to the polarization perpendicular to the wave vector of the spiral structure, just as in equation (3). This DMI stabilization of the electric displacement is completely independent of the crystal structure, while the theory described by Mostovoy[6] is only valid for cubic crystal structures.
Concluding, the interaction between the magnetic ordering and the ferroelectricity in these materials is caused by the combination of the spiral spin density wave, the DMI interaction and the atomic displacement.

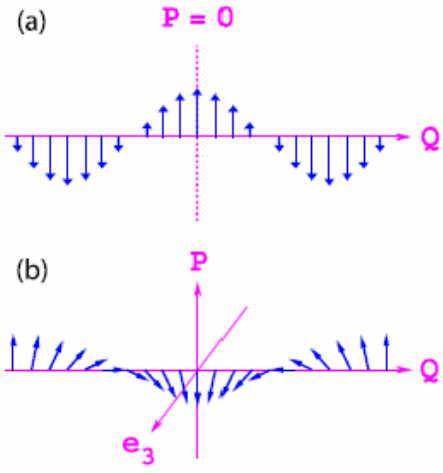

Figure 2: The sinusoidal spin density wave gives rise to local polarizations but the average polarization is zero (a). For the helical spin density wave the average polarization is nonzero and perpendicular to the spin rotation axis and the wave vector (b). Picture was taken from ref. 6.

Chapter 3: FeS

3.1 Introduction

Research on multiferroics has been ongoing since the 1960s. In 1982, Smolenskii[1] et al. wrote a review on the ferroelectric materials that were known up to that moment. They mentioned the perovskites, the hexagonal rare earth manganites, the Bi compounds and the materials of the $BaMF_4$ class (M=Mn, Fe, Co, Ni). Besides these well established multiferroics the paper also discusses FeS as a possible candidate for multiferroicity.
FeS (troilite) has a hexagonal structure and is known to be an antiferromagnet below the Néel temperature at 600K. At 400K the magnetic susceptibility shows an anomaly which is attributed to a reorientation of the magnetic easy axis. At this transition van den Berg et al.[8] reported to have measured a triple peak in the pyroelectric current, as is shown in figure 3. They claimed to have observed hysteresis loops in the polarization at temperatures lower than 400K. The observed polarization varied between 1000 - 7000 $\mu C/m^2$ and strongly depended on the applied electric field as is summarized in table 1. Moreover, the polarization was only observed in the c-direction.

Table 1: Polarization data for FeS taken from [8].

Applied field (KV/cm)	*Polarization ($\mu C/m^2$)*
2.6	1000
3.8	2000
4.4	2500
5.8	4000
8.0	7000

The observations by van den Berg were subject to a great discussion, because the low temperature phase was thought to be of the centrosymmetric space group P-62c and thus the material could not be a ferroelectric. However in 1996 Li et al.[17] did a study on FeS that involved DTA and x-ray diffraction measurements. They argued that, on the basis of their x-ray and DTA results, the x-ray patterns could as well be interpreted as being consistent with the P31c space group, which is noncentrosymmetric. Thus, the statement by van den Berg about the ferroelectricity in FeS might be accurate.

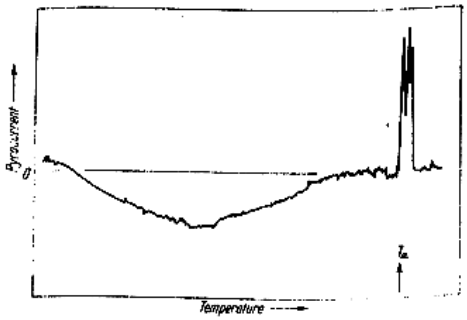

Figure 3: The pyroelectric current that was measured by van den Berg et al.[8]. The current appeared approximately at the alpha transition at 400K.

Moreover the recent developments in the field of multiferroics suggest that multiferroicity can be observed for a very broad range of materials. For example the recent theory on ferroelectricity induced by magnetic ordering could shed some light on the observations in FeS, as this material also has coinciding magnetic and electric transitions.
This chapter of the report will therefore be focused on the question of whether FeS is indeed a multiferroic. First, a short introduction will be given on the crystallographic and magnetic structure of FeS. Next, the crystal synthesis and details of the experimental measurements will be described. In the fourth section, the results of the x-ray diffraction, magnetization, resistivity and heat capacity measurements will be discussed. The last part of this chapter will be dedicated to a discussion on how the results should be interpreted and which questions still need to be answered.

3.2. Magnetic and crystallographic structures of FeS

During the last hundred years a lot of research has been done on iron sulfide compounds. These compounds can appear in many different stable phases for different iron stoichiometries $Fe_{1-x}S$. The possible structures are summarized in a phase diagram in figure 4.

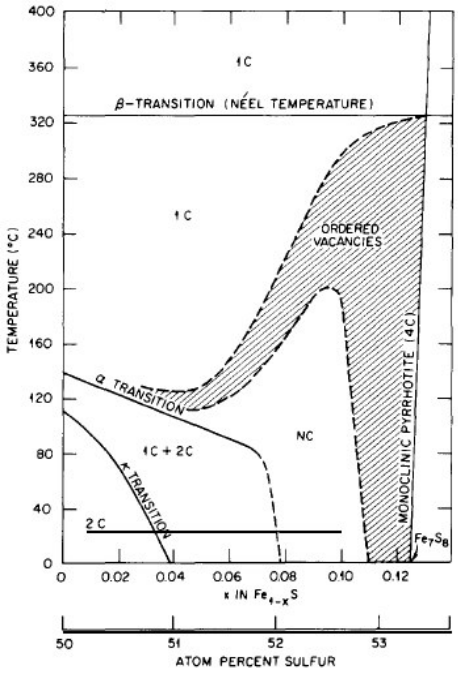

Figure 4: phase diagram of FeS, taken from van de Berg[18]

A composition independent phase transition takes place at 328 °C. At this temperature the high temperature paramagnetic phase is transformed to the low temperature antiferromagnetic phase. This temperature is often called the Néel temperature, but in most literature concerning FeS, it is referred to as the β-transition. For $x < 0{,}04$ the material is hexagonal but when the iron content decreases the structure becomes

monoclinic. However, for many compositions a mixture of both phases is observed. As a result of the lower iron content, the phases with x >0.04 can contains an ordered arrangement of the vacancies. In this regime, indicated by the hatched area, several different space groups occur. Due to the ordering of the vacancies, some of the phases in this area are ferrimagnetic.

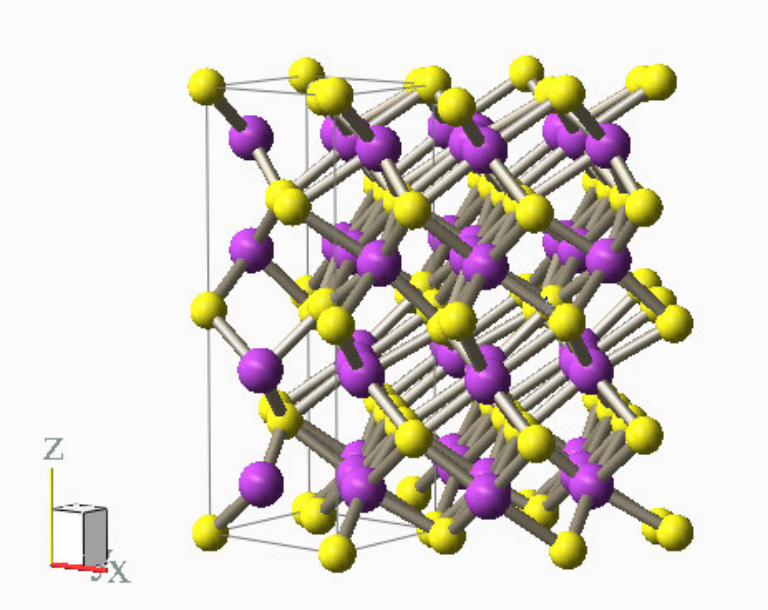

Figure 5: The crystal structure of FeS in which Fe is purple and S is yellow. The Fe atoms are surrounded by an octahedron of sulfur atoms.

In the stoichiometric composition, where the same amount of sulfur and iron atoms are present, the iron sulfide crystallizes in a hexagonal structure as is shown in figure 5. The Fe^{2+} ions are surrounded by a octahedron of sulfur atoms. At temperatures above the alpha transition (400K) the FeS has the space group $P6_3/mmc$. Below the alpha transition the octahedron becomes distorted and the unit cell doubles. Therefore the high temperature phase is often referred to as the 1C phase and the low temperature phase as the 2C phase. The space group of the 1C phase is subject to controversy; both centrosymmetric P-62c[19] and non-centrosymmetric P31c[17] are said to fit the x-ray pattern. In addition, King et al.[20] suggested that the high temperature phase between the alpha transition and the Néel temperature has a different structure than that above the Néel temperature, namely the Pnma structure which is often referred to as the MnP phase. This statement is not at all generally accepted.

In FeS the only magnetic components are the Fe^{2+} ions. These ions have 6 d-electrons in the high spin configuration and thus S=2. The stoichiometric FeS is an antiferromagnet below the Néel transition. In the same temperature range as the alpha transition a spin flip transition is present in which the magnetic moments turn from lying in the a-b plane above the transition to point along the c-axis below. This transition does not occur at exactly the same temperature as the structural transition, but it is expected that both transitions are strongly correlated. The transition temperature strongly depends on the composition of the FeS.

3.3. Experimental

Iron sulfide powder was synthesized by mixing stoichiometric amounts of Fe powder and sulfur. The mixture was sealed under vacuum in a quartz tube by heating one end of the tube while the enclosed part of the tube was cooled in liquid nitrogen. Subsequently, the tube was placed in a furnace at 900°C for 74 hours. Two different techniques were used to synthesize the crystals, the Bridgemann technique and the vapor transport technique. In the Bridgemann[21] technique the FeS powder was again sealed in a quartz tube under vacuum. The tube was slowly (5mm/hour) pulled through a vertical furnace which was at 1200°C. This method was unable to melt the material completely, as the maximum temperature of the oven (1200°C) was just around the melting point of FeS. However the synthesis resulted in an ingot that consisted of small shiny crystals of about 1x1x1mm.

For the vapor transport method the FeS powder was placed in a larger quartz tube together with a small amount of NH_4I (1.5mg/ml)[22]. The quartz tube was placed in a temperature gradient as is shown in figure 6. The FeS powder and the NH_4I were placed at the hot side of the tube (batch 1: 950°C, batch 2: 900°C) resulting in the following reaction:

$$2\ NH_4I\ (g) + FeS(s) \rightarrow FeI_2\ (g) + H_2S\ (g) + 2\ NH_3\ (g)$$

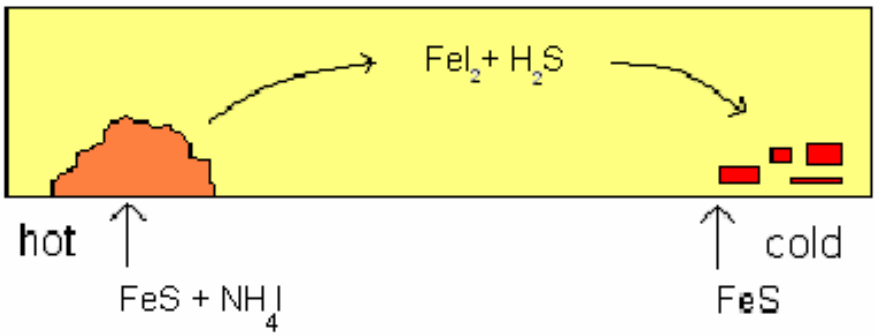

Figure 6: The synthesis set up for the vapor transport growth.

At the cold side (batch 1: 900°C, batch 2: 800°C) of the tube the equilibrium lies on the other side and so FeS is formed, resulting in crystal growth. The first batch was grown using a different temperature gradient than the second batch of crystals. After 2 weeks both batches showed crystals with a maximum size of 3x3x3mm that are shown in figure 7. As these crystals were much bigger than the Bridgemann crystals, only vapor transport crystals were used in the experiments.

To characterize the synthesized materials, X-ray diffraction was preformed on the powder (Bruker d8 K_α Cu radiation) as the crystals (Bruker Smart Apex CCD K_α Mo radiation and Enraf Nonius CAD4 K_α Mo radiation). The powder patterns were refined with GSAS[23] and for the single crystal patterns SHELXTL was used. The different phase transitions were studied by measuring the specific heat using a DSC-TGA (TA instruments). The electric properties of the FeS crystals at low temperatures were determined on the Quantum Design Physical Properties Measurement System (PPMS).

At temperatures above room temperature a Radiant Precision Workstation was used in combination with an Agilent LCR meter. The magnetic properties were determined using a Quantum Design Magnetic Properties Measurement System (MPMS).

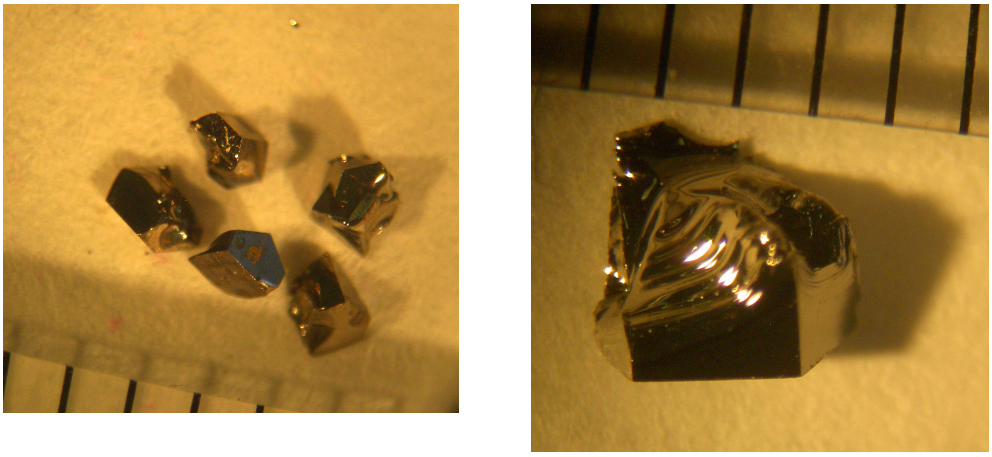

Figure 7: The crystals that were obtained by the vapor transport crystal growth method.

3.4 Results

X-ray diffraction was performed on single crystals and crushed single crystals to investigate the purity of the material and to determine the space group. The powder diffraction experiments showed that the peak positions were consistent with those reported before. Thus it could be concluded that the crystals were indeed FeS. The peak intensities, however, were difficult to fit due to overlapping peaks in the pattern. Single crystal diffraction allowed more straightforward refinements to be carried out. From the shape of the crystals it was already clear that the material was hexagonal and thus the pattern was refined with both the P-62c and the P31c space groups. The lattice parameters for the vapor transport crystals (batch 1) were found to be a=5.9828(5) and c=11.7530(8). The atomic positions and isotropic temperature factors obtained from both refinements are given in table 2.

Table 2: Atomic positions and isotropic form factor for Fes.

		x	***y***	***z***	***U***
P-62c	Fe	0.3732(2)	0.0486(3)	0.1232(6)	0.0166(3)
	S1	0.0000(-)	0.0000(-)	0.0000(-)	0.0091(5)
	S2	0.3333(-)	-0.3333(-)	0.01822(19)	0.0121(4)
	S3	0.6653(3)	-0.0023(4)	0.2500(-)	0.0092(5)
P31c	Fe1	0.3730(2)	0.0483(3)	0.12325(8)	0.0170(4)
	Fe2	0.0484(3)	0.3730(2)	-0.12325(8)	0.0168(4)
	S1	0.0000(-)	0.0000(-)	0.0006(4)	0.0090(4)
	S2	0.3333(-)	-0.3333(-)	0.0183(3)	0.0122(8)
	S3	0.6667(-)	0.3333(-)	-0.0180(3)	0.0117(7)
	S4	0.3325(2)	0.3349(2)	0.2500(4)	0.0089(3)

Table 3: Refinement results for the single crystal x-ray diffraction patterns.

	P-62c	***P31c***
Number of reflections	393	734
Number of refined parameters	21	37
wR(F^2) = $[\sum [w(F_o^2 - F_c^2)^2] / \sum [w(F_o^2)^2]]^{1/2}$	0.1367	0.1162
R(F) = $\sum (\|\|F_o\| - \|F_c\|\|) / \sum \|F_o\|$	0.0483	0.0450
GooF = S = $[\sum [w(F_o^2 - F_c^2)^2] / (n-p)]^{1/2}$	1.134	1.449
Difference Fourier map **e/Å^3**	-0.7 2.4	-1.1 1.4

The results of the refinements for both space groups are shown in table 3. The definitions of the weighting parameters used are given in the table, where F_0 and F_c are the observed and calculated structure factor amplitudes, n is the number of reflections and p is the number of refined parameters. The R-values were compared by making use of the Hamilton test[24]. In this test the ratio of the two R-values is T.

$$T=R_{constrained}/R_{unconstrained}$$

In this equation $R_{constrained}$ is the R-value for the refinement with the least variables (P-62c) and $R_{unconstrained}$ the R-value for the refinement with the most variables (P31c). In the paper of Hamilton it is mentioned that the weighted R values should be used and not the normal R. One finds T=1.1764. Now we can make the following hypothesis: "P-62c gives a better fit to the measured pattern than P31c".
This is true as long as: $T<R_{b,n-m,a}$
These $R_{b,n-m,a}$ are reference values that are tabulated in the mentioned paper with respect to the number of reflections (n), the number of variables in both cases(b and m) and the significance level at which the hypothesis can be rejected or accepted (a). For this situation b=37-21=16, n-m=393-16=377. For different significance levels we find listed R values of (see tables in the paper):

a=5% R<1.1092
a=2.5% R<1.1204
a=1% R<1.1346
a=0.1% R<1.1457

Thus $T> R_{b,n-m,a}$ for all these significance levels, which means that the hypothesis can be rejected at a significance level of 0.1%. Thus, according to this calculation, the space group is almost sure to be P31c. However, slight changes in the refinement can influence the R factors drastically and thus one should be very careful while interpreting these results.
The temperature dependence of the lattice parameter through the alpha transition was measured both for the powder and for the single crystals. The change in powder diffraction patterns is shown in figure 8. The arrows mark the (101) (201) and (211) reflections that disappear when the temperature increases.

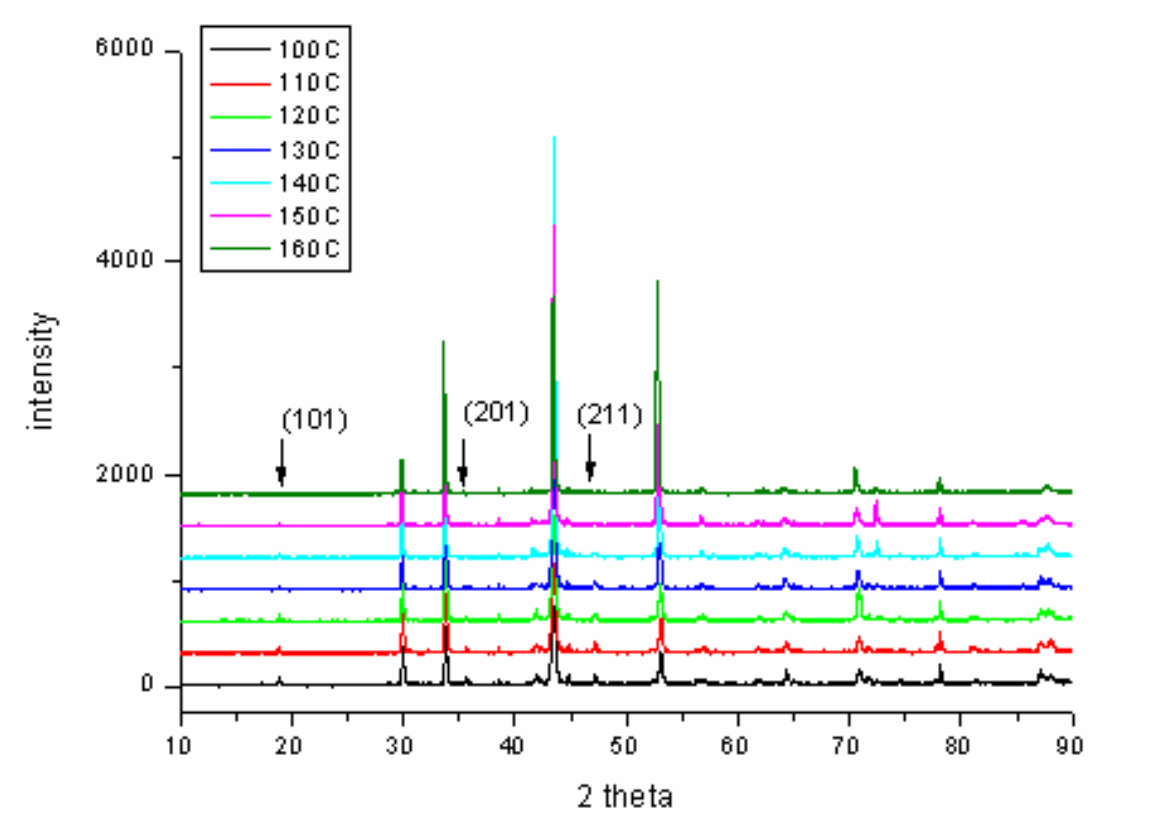

Figure 8: The temperature dependence of the powder diffraction patterns around the alpha transition. The peaks of the doubled cell, which are marked by the arrows, are disappearing when the material goes through the phase transition.

As the temperature increases, FeS is transformed from the 2C to the 1C phase, in which the unit cell becomes half as big. The (hkl) reflections with l=odd disappear. The transition from the 2C to the 1C phase seems to go gradually within the temperature range of 120-140°C. Although the change in diffraction patterns is clear it was very hard to refine these patterns in a meaningful way.

During the alpha transition the lattice parameters were also monitored with single crystal diffraction on the CAD4 diffractometer. Clear transitions were observed in the lattice parameters around 90°C. The a and b lattice parameters increase and the c parameter decreases both by approximately 1 %, as is shown in figure 9. The single crystal data above the alpha transition could be refined with the P63/mmc space group reported by Collin[19] but not with the Pnma space group suggested by King[20]. The observations differ from the other crystal and powder diffraction measurements in two ways. First, the transition temperature is much lower than that observed using powder diffraction. Second, the lattice parameters measured at room temperature with the CAD4 (a=5.96(2)Å c=11.67(5)Å) are somewhat smaller than those observed with the Apex single crystal diffractometer (a=5.9828(5)Å c=11.7530(8)Å). These differences might be due to the composition of the samples, as they came from different batches.

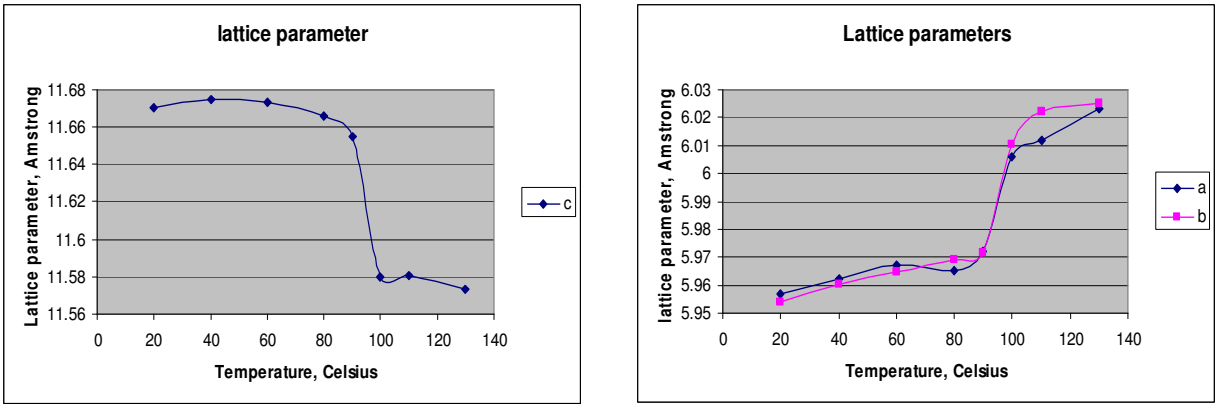

Figure 9: Temperature dependence of the lattice parameters determined using the CAD4 diffractometer. The lattice parameters show a jump at around 9°C of approximately 1%.

The difference in transition temperature may also be caused by the CAD4 heating system, because it measures temperature 5 mm from the crystal and thus the difference between the actual temperature and the measured temperature can be large.
As already mentioned in the introduction, many different compositions are possible for FeS. The x-ray results show that the crystals are hexagonal, but the refinements were unable to give an accurate estimate of the actual composition. The refinement using the diffraction data from the Apex resulted in a composition between stoichiometric FeS and FeS with 2% excess of sulfur. In a paper from Perthel[25] however a correlation was reported between the lattice parameters and the relative sulfur content. The values of 11.7530(8)Å and 11.67(5)Å would correspond to stoichiometric FeS and FeS with 2% excess of sulfur.
In order to distinguish between the P-62c and P31c space groups at room temperature, Raman spectroscopy on the surface of a FeS crystal was attempted. Because the P31c space group is lower in symmetry, one would expect to see more Raman modes than for the P-62c space group.

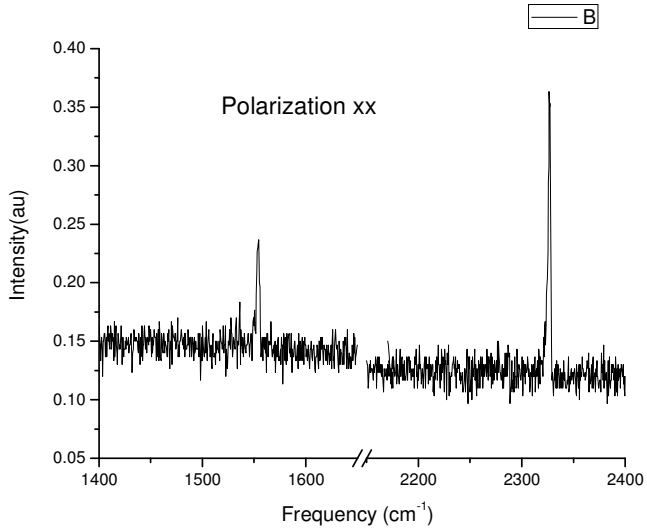

Figure 10: The Raman spectrum of FeS in the zz polarization.

The easiest way investigate this is to measure the fully symmetric modes in the zz polarization. P62c should have just 5 active modes, while P31c should have 11. In the Raman spectra, however, only two peaks were observed, as is shown in figure 10. Both space groups could give rise to these peaks, so on the basis of these measurements one can not conclude anything. For the other polarization directions no reflections were observed. This could be due to the high (metallic) reflectivity of the sample, which allowed only a little light to penetrate the material.
The heat capacity was measured between room temperature and 450 °C. With increasing temperature two peaks were visible (figure 11) for the crystals grown in batch 1; one at 120°C (alpha transition) and one at around 300°C (Néel temperature). On cooling the Néel temperature peak was still present but the alpha transition anomaly was not seen. It was observed that the material broke down at temperatures above 500K, as the transitions disappeared when a sample was heated above this temperature. Because no significant change in the weight could be observed, the cause of the disappearance of this feature is still unclear. The measurement could be reproduced for crystals that were grown in batch 2, but the temperature at which the first transition appears differs; the alpha transition is around 370K. This is probably due to composition differences between the crystals in the two batches. The transitions that were observed in the x-ray experiments show the same differences in temperature between the two batches. For crystals, within one batch the transition temperatures were identical.

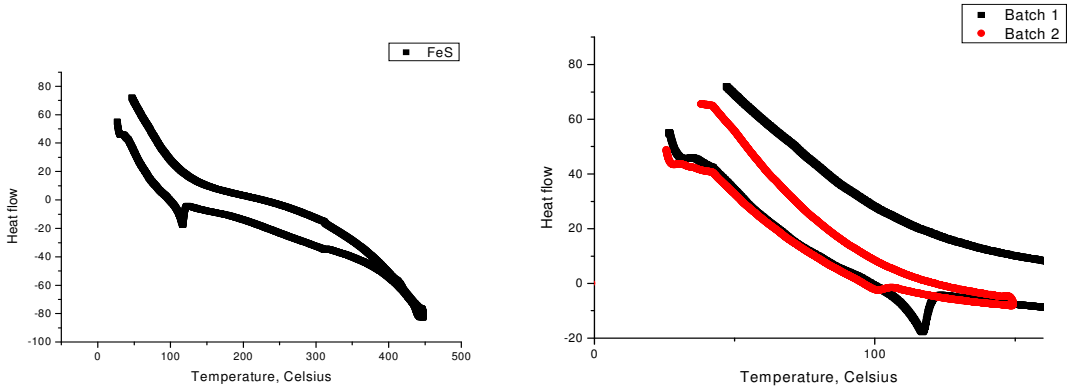

Figure 11: The heat capacity measured for the two batches of FeS.

Unfortunately the equipment used to measure magnetization at elevated temperatures did not function and therefore only the magnetic properties below room temperature were measured. Although these measurements are not relevant for characterizing the alpha transition, they revealed an anomaly that has never been reported before. The magnetization is shown in figure 12 for magnetic fields applied along c and perpendicular to c. Both measurements show an anomaly at approximately 160 K, which could be reproduced for both batches. The origin of this transition is not known. It might be that due to a change in composition the spin flip temperature has shifted from 400K to 160K. However, as the heat capacity and the x-ray data show that the alpha transition has not shifted more than 40 degrees, it is not very likely that the spin flip transition would have changed so much for these crystals.

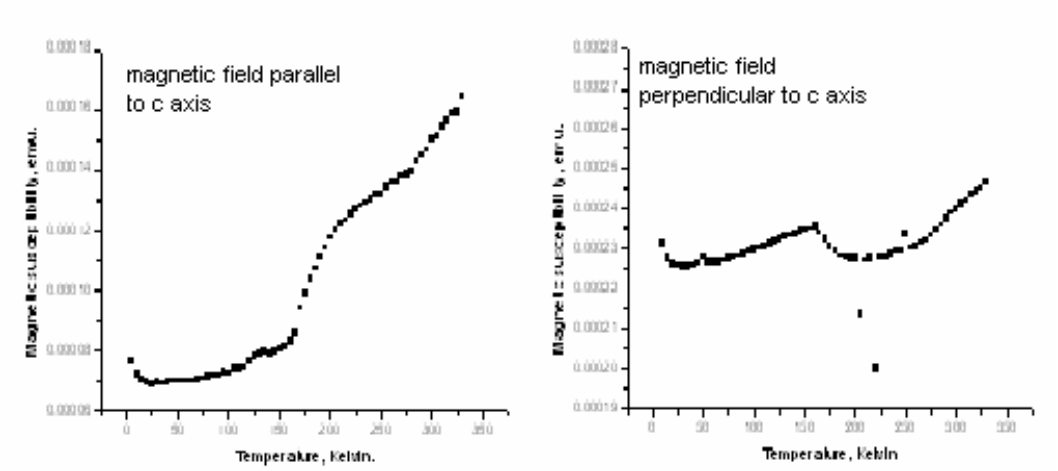

Figure 12: The magnetization for FeS at low temperatures in a field of 100 Gauss. The crystals were cooled in zero field. An anomaly was observed around 160K for both crystal batches. The origin of this transition is still unknown.

The magnetic moment per formula unit was calculated from the magnetic susceptibility and the mass of the crystal to be approximately $1x10^{-3}$ bohr magneton. Besides, the magnetic susceptibility increases with temperature, thus the transition can only be between two antiferromagnetic structures.

Two point resistance measurements were carried out on the iron sulfide crystals of batch 1. The low temperature behavior is semiconductor-like as is shown in figure 13a. At the alpha transition a drop in resistance is observed, see figure 13b. These measurements are two point measurements along the b direction and thus the absolute values are including the contact resistance. It was difficult to perform 4-point resistance measurements in this crystallographic orientation because the plane parallel to the c axis was not at all flat. Perpendicular to the c-axis, 4-point resistivity could easily be measured. A resistivity of approximately 80 Ohm*m at room temperature was obtained, which is of the same order of magnitude as was earlier reported by Coey et al.[26] The conductivity was too high for poling to be performed and with the virgin crystal no pyroelectric current could be observed. The noise of the set-up was rather high (5-10 pA) and thus it could be that the signal was not high enough to overcome the noise.

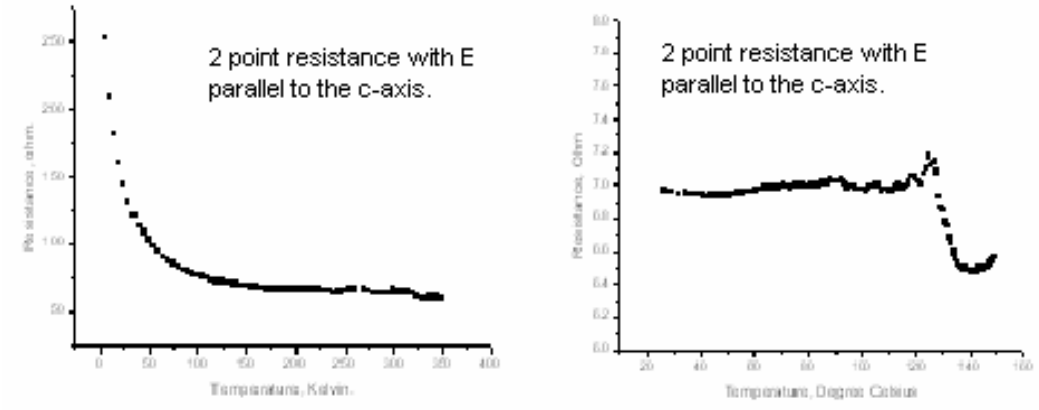

Figure 13a (left): The resistivity versus temperature shows a semiconductor like behavior.
Figure 13b (right): At the alpha transition a drop in the resistivity is observed along the c-axis.

3.5.Discussion and Conclusion

The vapor transport method resulted in FeS crystals up to 3x3x3mm. The room temperature x-ray diffraction data showed that the crystal structure has the noncentrosymmetric space group P31c instead of the centrosymmteric P-62c. The x-ray and heat capacity measurements show a clear transition at 400 K for the crystals from batch 1. The crystals from batch 2 show a similar transition at the lower temperature of 370 K. This difference in transition temperature is probably due to differences in the stoichiometry of these two types of crystals. From the x-ray diffraction patterns it could be deduced that batch 1 contains stoichiometric FeS and batch 2 has a 2% excess of sulfur. These changes in composition are due to the differences in crystal growth.

The alpha transition results in the disappearance of peaks in the x-ray pattern which confirms the doubling of the unit cell on cooling through the phase transition. The high temperature phase was found to be consistent with the P63/mmc structure. A sudden change in the lattice parameters was observed at the alpha transition.

Due to the breakdown of the high temperature setup of the MPMS no magnetization data were obtained at the alpha transition. However, the low temperature magnetization data showed an anomaly at 160K, which might also be worth some attention as no magnetic transition has ever been reported at this temperature. The resistance of FeS shows a temperature dependence that is consistent with semiconducting behavior. At the alpha transition a drop in resistivity is observed. The resistivity of 80 Ohm*m, however, is to low to perform any dielectric or pyroelectric measurements. Other multiferroics normally have a resistivity of 10^5 Ohm*m or higher. Thus, no answer can be given to the question of whether FeS is ferroelectricity or not.

Chapter 4: $MnWO_4$

4.1. Introduction

This chapter will be focused on the magnetic and dielectric properties of $MnWO_4$. The magnetic structure of $MnWO_4$ is known to be frustrated below the Néel temperature of 13.5 K. This frustration leads to the appearance of several uncommon magnetic structures. At low temperatures the structure is an antiferromagnet with an up-up-down–down structure along the a axis. Above 8 K the magnetic ordering is transformed into a long period helical spin density wave. According to the theory developed by Mostovoy [6], which was discussed in chapter 2, this spiral magnetic structure is expected to give rise to a polarization perpendicular to the spin rotation axis and the incommensurate wave vector. Thus this spiral magnetic structure in $MnWO_4$ is expected to be ferroelectric and antiferromagnetic. The research presented in this chapter in focused on the characterization of this predicted multiferroic.

In the next section the crystallographic and magnetic structure of $MnWO_4$ will be reviewed. The third section will discuss the synthesis of the $MnWO_4$ crystals and the experimental procedures. In the fourth section the results of the x-ray diffraction, heat capacity, magnetization, dielectric constant and pyroelectric current measurements will be presented. In the fifth section the results will be discussed in relation to the theory and other materials that show ferroelectricity induced by magnetic ordering. In the last section this research will be discussed in the context of the recent developments in the field of multiferroics. It will be explained how these results could contribute to the understanding of multiferroic materials and the magnetoelectric effect and which questions still need to be answered.

4.2. Structure and magnetic order in $MnWO_4$

The structure of $MnWO_4$ (figure 14) crystallizes in the wolframite structure that is also observed for other transition metal tungstates like $FeWO_4$ and $CoWO_4$. This structure consists of successive layers of Mn^{2+} and W^{6+} ions, which are both surrounded by a distorted octahedron of oxygen atoms. The octahedra form zigzag chains along the c axis.

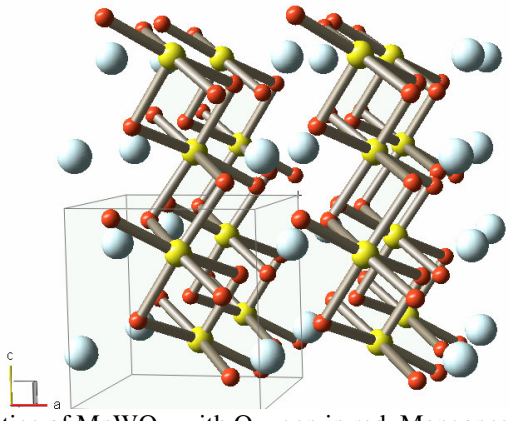

Figure 14: the crystal lattice of $MnWO_4$, with Oxygen in red, Manganese in yellow and tungsten in blue.

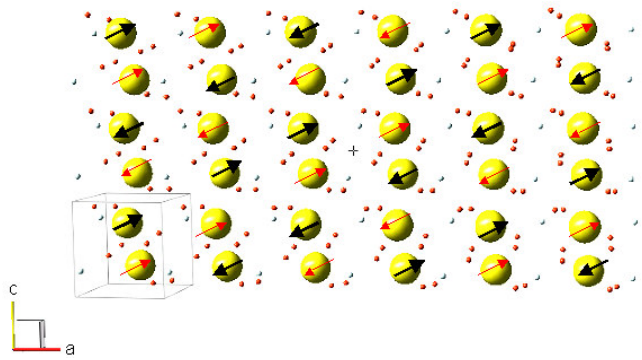

Figure 15: The magnetic structure of $MnWO_4$ in the AFM1 phase. The red and the black spins represent the two different sub lattices as proposed by Dachs[31].

The oxygen atoms form a hexagonal closed packed structure, and the tungsten and manganese ions occupy only half of the octahedral sites. The crystal adopts the monoclinic space group P2/c.

Below the Néel temperature at 13.5 K $MnWO_4$ displays several magnetic structures. The magnetic phase below 6-8 K is called AFM1. It is reported [27] [28] to have a propagation vector of (-¼, ½, ½) with respect to the chemical cell, and shows an up-up-down-down kind of magnetic order along the a-direction (see figure 15). In this structure the magnetic unit cell is 16 times bigger than the crystallographic unit cell and the symmetry can be described by the P_C2/c magnetic space group. When the temperature increases the magnetic structure transforms into a spiral with the propagation vector (-0.2165, ½, 0.4585). This structure is called the AFM2 structure. Above 12.5K the magnetic structure transforms again to a sinusoidal state, which will be called the AFM3 from now.

Above 13.5 K the system becomes paramagnetic. In all these magnetic structures the magnetic easy axis lies in the a-c plane making an angle of 35° with the a axis. The easy axis will be referred to as the x axis. The magnetic y axis is the same as the crystallographic b axis and the third magnetic axis, z, is perpendicular to both the x and the y axes.

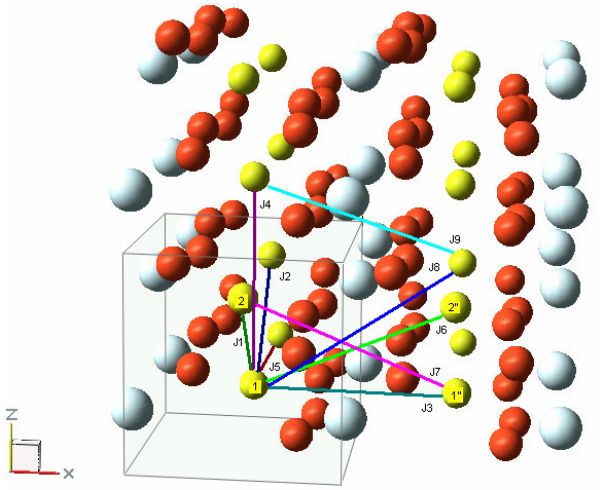

Figure 16: The crystal structure of $MnWO_4$ with Mn: yellow, O: red and W: light blue. The colored lines represent the magnetic interactions.

The only magnetic component in $MnWO_4$ is Mn^{2+}. It has five d electrons in the high spin configuration and thus the angular momentum of one ion is 5/2.The Mn^{2+} ion has nine different Mn^{2+} neighbors. The magnitude and sign of the interactions between these ions are determined by Ehrenberg et al.[28] by means of inelastic neutron experiments. Their results are given in table 4 and visualized in figure 16. In this figure the Mn^{2+} ions are in yellow, the oxygen atoms in red and the tungsten in light blue. The separation between the magnetic ions is rather large and therefore no direct interactions are possible [29]. All interactions are intermediated by one or more oxygen or tungsten atoms via 90˚ and 180˚ superexchange interactions. Therefore the strength of the exchange interaction does not depend on the distance between the interacting ions. Instead the interaction depends on the number of d electrons on the ion, the configuration of the spins (high or low spin) and the angle between the manganese ions and the intermediating atoms[30]. In the AFM1 phase the interaction between atom 1 and 1" (J3) is frustrated and this leads to the up–up–down–down structure along this axis. Different explanations for this frustration have been given. Lautenslager et al. [27] assumed that the superexchange (Me-O-O-Me) interaction J7, interaction J6 and J1 are the dominant ones. They found that J7<0, J6>0 and J1<0, and so the combination of J6+J1 would lead to an antiferromagnetic coupling between atom 1 and 1", but the interaction J1+J7 would induce a ferromagnetic coupling between these two atoms. This results in a frustration that will be reduced in the up-up-down-down structure. Although the data published by Ehrenberg give different values for these interactions they do lead to a frustration between 1 and 1''.

Table 4: The magnetic exchange interactions in $MnWO_4$ as proposed by Ehrenberg et al.[28].

	Position neighbor	***Distance Å***	***Exchange coupling***
	(½, 1-y, ¾)	3.283	-0.195
J1	(½, 1-y, -¼)		
J2	(½, 2-y, ¾)	4.398	-0.135
	(½, 2-y, -¼)		
J3	($^3/_2$, y, ¼)	4.823	-0.423
	(-½, y ¼)		
J4	(½, y, $^5/_4$)	4.992	0.414
	(½, y, -¾)		
J5	(½, y-1, ¼)	5.753	0.021
	(½, y-1, ¼)		
J6	($^3/_2$, 1-y, ¾)	5.795	-0.509
	(-½, 1-y, -¼)		
J7	(-½,1-y, ¾)	5.873	0.023
	($^3/_2$, 1-y, ¼)		
J8	($^3/_2$, 2-y, ¾)	6.492	0.491
	(-½, 2-y, -¼)		
J9	(-½, 2-y, ¾)	6.561	-1.273
	($^3/_2$, 2-y, -¼)		

The interaction between these atoms is strongly antiferromagnetic (J3 = –0.423) and the interaction is even strengthened via the J1 and J7 interactions. However the J6 interaction is antiferromagnetic so that this interaction opposes the J3 and J1+J7 via the J1 interaction between 1'' and 2''. Many other interactions are possible that lead to a frustration of this kind, for example the interaction J4+J9+J2 will lead to a ferromagnetic coupling between 1 and 1', while the interaction J8+J2 again leads to an antiferromagnetic coupling between these two ions. Hans Dachs [31] however uses quite a different approach to explain this frustration. The theory he describes in based on the presence of two different sub lattices that have a strong coupling between the atoms within one lattice but only a weak interaction with the atoms from the other sub lattice. The sub lattices are represented by the red and black arrows in figure 15. Within one sub lattice the interactions between the magnetic components are given by:

$$E = J_{11'} - J_{12} + J_{13} + J_{23} \qquad (4)$$

Where $J_{11'}$ is the interaction between atom 1 and the atom "behind" it, 1'.The coupling between the two sub lattices arises from an interaction between 1, 1' and 4 that makes 4 parallel to both 1 and 1'; inducing the up-up-down-down structure.
The crystal structure of $MnWO_4$ is similar to other tungstenates like $MeWO_4$ (Me=Fe, Co, Ni). The magnetic structure, however, is very different. The $MeWO_4$ (Me=Fe, Co, Ni) all show a regular antiferromagnetic order[32]. For these materials, the number of d electrons is higher than for the Mn^{2+} ion and this changes the superexchange in such a way that the frustration does not appear in these materials.

4.3. Experimental

The $MnWO_4$ crystals were synthesized by making use of two different crystal growth techniques; the flux growth technique and the floating zone method. In the flux growth technique stoichiometric amounts of the starting materials $MnCO_3$ and WO_3 were mixed together with an excess of Na_2WO_4 that functioned as the flux material. The mixture was placed in a platinum crucible and heated up to 1250 ºC from which it was slowly (1ºC per hour) cooled to 600ºC [33]. The crystals were removed from the flux by dissolving the flux material into a NaOH solution. This method resulted in black crystals of approximately 2x2x2mm, which are shown in figure 17.
For the floating zone technique, $MnWO_4$ powder was first synthesized by calcination of MnCO3 and WO_3 at 1050ºC for 60 hours in a N_2 gas flow. The resulting light brown powder was pressed into a rod, which was used in the floating zone set up.

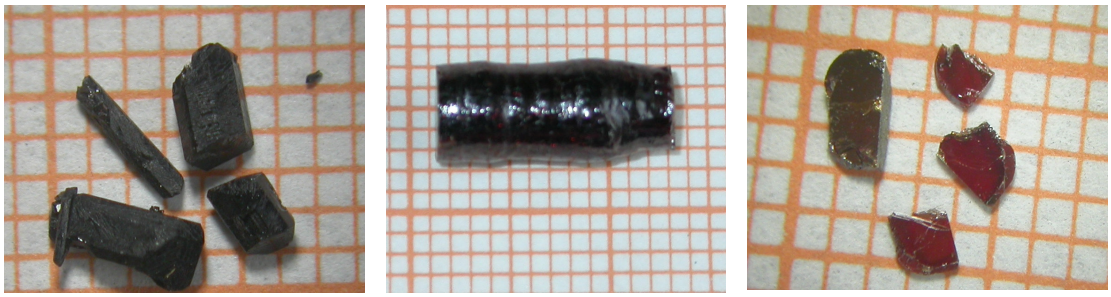

Figure 17: Flux grown crystals (left), and the floating zone crystals (middle and right).

The rod was pulled through the hot zone at a speed of approximately 5-7 mm per hour in an atmosphere of nitrogen. The obtained crystals were as large as 5x5x5 mm and they were transparent red brown in color. The crystals could easily be cleaved perpendicular to the b axis.
Both types of crystals were characterized by powder x-ray diffraction by making use of a Rigaku miniflex powder diffractometer. The diffraction patterns were refined with GSAS [23] to determine the purity of the crystals. The heat capacity of both types of crystals was measured, using a Quantum Design Physical Properties Measurement System.
For the magnetic and dielectric measurements only the floating zone crystals were used. The crystals were cut, polished or cleaved to create the desired surfaces. Subsequently, contacts were made by sputtering gold on the surfaces. The crystals with the gold contacts were annealed at 400 ºC in air for 2 hours. To connect this crystal to the measurement probe silver paint, gold- and copper wires were used. The measurements were done on a Quantum Design Physical Properties Measurement System (dielectric and pyroelectric) and a Quantum Design Magnetic Properties Measurement System (magnetic properties).

4.4. Results

For both the flux grown and the floating zone crystals x-ray diffraction patterns were taken at room temperature. The x-ray diffraction pattern of the flux grown crystals showed one peak at 32.9 (2 theta), which could not be assigned to the $MnWO_4$ structure. This peak was caused by a pollution of Mn_2O_3, estimated to be a few mol percent. The diffraction pattern of the floating zone crystals contained only peaks from the $MnWO_4$ structure. The material has space group P2/c with lattice parameters of 4.825, 5.755 and 4.993 Å and angles of 90, 91.138 and 90˚. The atomic positions and thermal displacement parameters are given in table 5. The final R-value of the refinement was 7.69 and the weighted R-value was 9.85; the fit is shown in figure 18. From the x-ray patterns it can be concluded that the floating zone crystals were more pure than the flux grown crystals, and so only floating zone crystals were used for the magnetic and electric measurements.

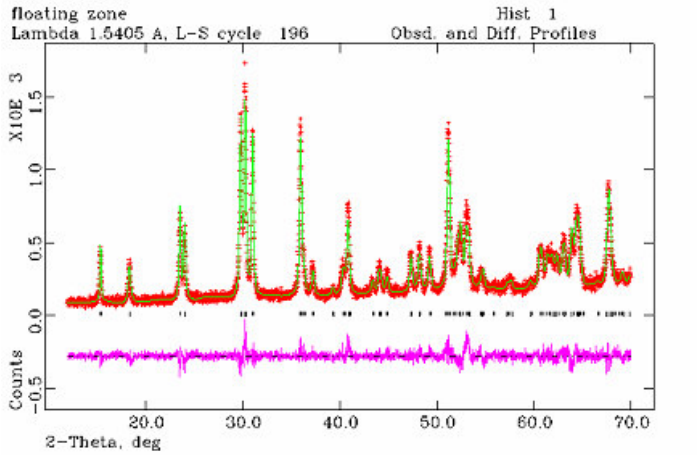

Figure 18: The diffraction pattern of the $MnWO_4$ (red) and the calculated profile(green). The pink line is the difference between the diffraction pattern and the fit.

Table 5: Atomic coordinates and isotropic temperature factors of the floating zone crystals of $MnWO_4$

	x	*y*	*z*	*U*
Mn	0.500	0.691	0.250	-0.0668
W	0	0.178	0.25	-0.0545
O_1	0.245	0.169	0.942	-0.0339
O_2	0.258	0.384	0.437	-0.0542

The specific heat was measured for both types of crystals to see how the impurity influences the phase transitions. The results are shown in figure 19. For the floating zone crystals the transitions in the specific heat are clearer than for the flux grown crystals, especially for the transition around 8 K. For the flux grown crystals this transition looks like a second order transition but the floating zone crystals show a clear first order transition. Moreover the transitions of the floating zone crystal are shifted to a higher temperature.

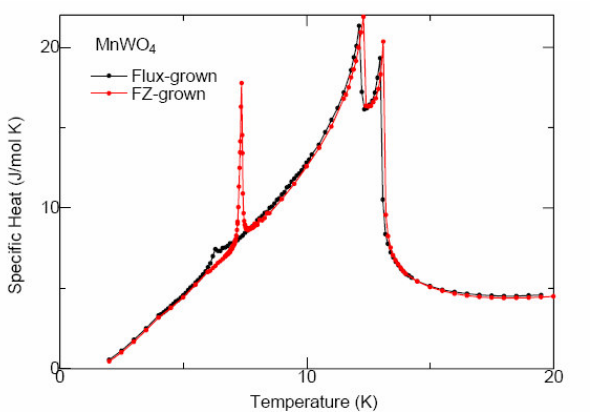

Figure 19: The specific heat for the flux (black) and the floating zone (red) crystals**.**

The impurities in the flux grown crystal that were observed by the x-ray experiments thus seem to weaken the transition towards the AFM2 phase. They also stabilize this AFM2 phase, as the transition temperature becomes lower. The peak at 8 K for the floating zone crystal is very sharp and therefore the transition is first order. The other peaks are weaker and look more like second order transitions. Because the transitions in the flux grown crystals seem to be altered due to the impurities, only floating zone crystals were used for the other experiments.

The magnetic susceptibility versus temperature was measured with the applied magnetic field along one of the magnetic axes. The results are shown in figure 20. When the external field (H) was applied along the y axis three transitions can be observed at 8, 12.5 and 13.5 K. Two of these transitions, at 8 and 13.5 K, could also be observed with the magnetic field applied along the x and z direction. From the observed transitions it can be concluded that four different magnetic structures are present in the measured temperature range. The phase below 8 Kelvin (AFM1) shows antiferromagnetic behavior[34]; The susceptibilities with the fields perpendicular to the easy axis are constant with respect to

temperature and the susceptibility with the external field applied along the easy axis shows a strong increase versus temperature. In the AFM2 phase, between 8 and 12.5 K, the susceptibility remains almost constant for the field applied along the x and z axes. Along the y axis an increasing susceptibility is present. In the AFM3 phase, between 12.5 and 13.5 K, the susceptibilities are the same as for AFM2 except for the case in which the field is applied along y. Thus the change from the AFM2 to the AFM3 phase only involves a change in the y component of the magnetization. Above 13.5 K the $MnWO_4$ crystal shows paramagnetic behavior along all magnetic directions.
The magnetic field dependence of the magnetic phase transitions shows a strong anisotropy. When the magnetic field was applied along the y or the z direction it hardly affected the temperature at which the phase transition occurred.

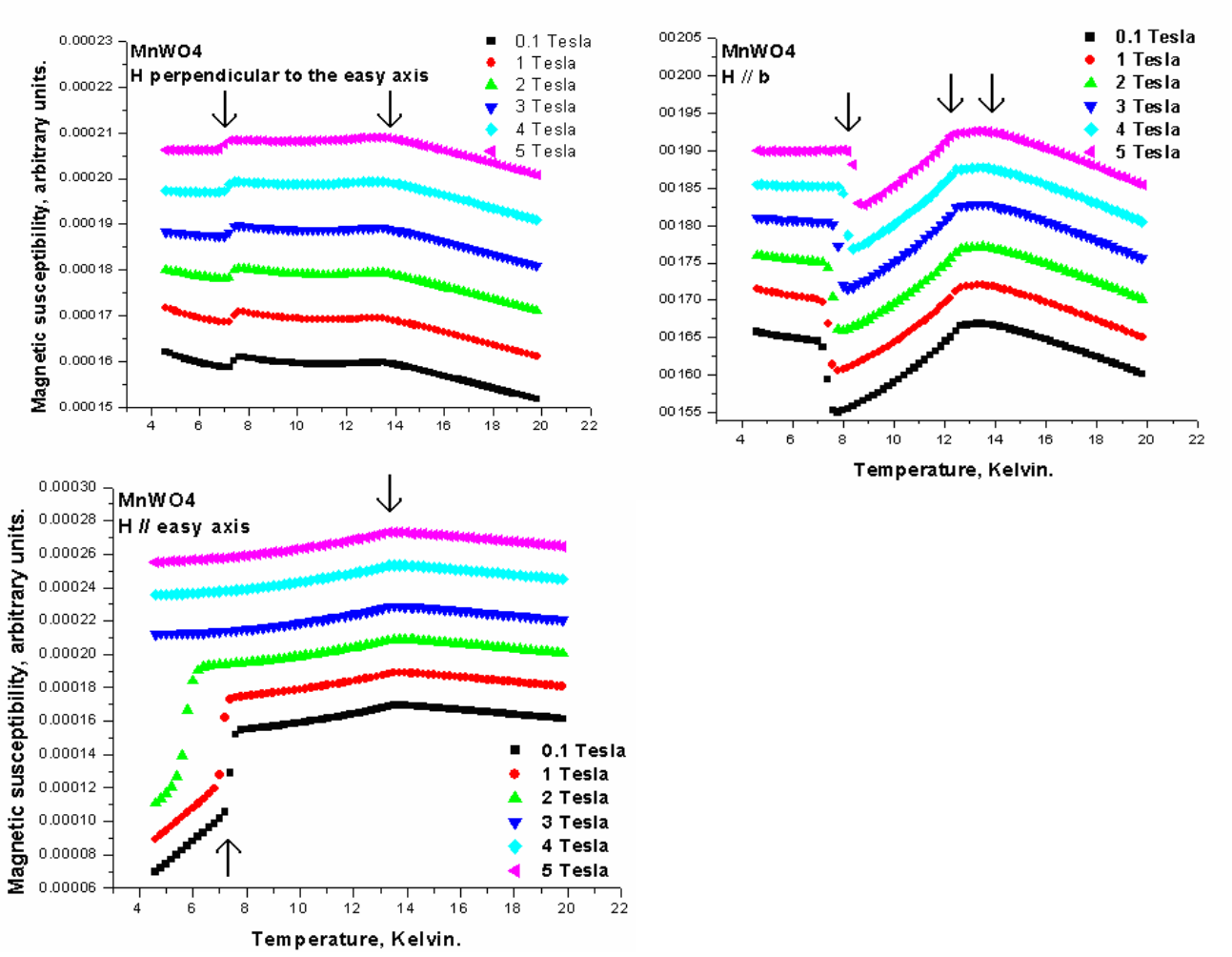

Figure 20: Magnetization versus temperature for the different directions of applied magnetic field: along the z (upper left), along the y axis (upper right) and along the easy (x) axis (lower).

However, with the magnetic field applied along the x direction (the easy axis), the transition from AFM1 to AFM2 shifts to a much lower temperature. From this observation it can be concluded that the AFM2 structure is stabilized by an applied magnetic field along the x axis.
In the paramagnetic phase, the magnetic susceptibility versus temperature shows ideal Curie –Weiss behavior, which means that the susceptibility behaves as:

$$\chi = C/(T+\theta) \qquad (5)$$

Where θ is the offset and C is the Curie constant. The fit of the measurement to the theory is shown in figure 21. The value found for θ was 75.6K. From the Curie constant the effective number of Bohr magnetons (p) was calculated to be 5.96. The theoretical value for p can be calculated by using the formula

$$p = g\,[J\,(J+1)]^{1/2} = 5.92 \qquad (6)$$

Where g = 2.0023 and J is the angular momentum quantum number which is 5/2 for a material with 5 unpaired spins. The theoretical value is very close to the measured value.

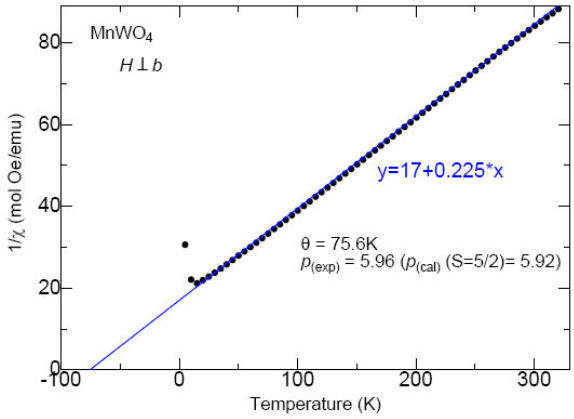

Figure 21: Above the Néel temperature the magnetic susceptibility (black dots) fits very well to Curie Weiss behavior (blue line).

In the same temperature range as the magnetic measurements, dielectric measurements were performed. In the dielectric measurements the electric field was applied along the y axis. Figure 22 shows the results for the 1 MHz measurement in the absence of a magnetic field. Two transitions are observed. The first anomaly appears around 8 K and shows a typical first order transition in the dielectric constant (see also the inset of figure 11). The second transition, at 12.5 K, looks like a second order transition. At this transition the dielectric constant behaves like a delta function; the dielectric constant before and after the transitions is equal but at the transition itself a sharp peak is observed.
The transitions in the dielectric constant appear at the same temperature as the magnetic transitions from AFM1 to AFM2 and from AFM2 to AFM3.

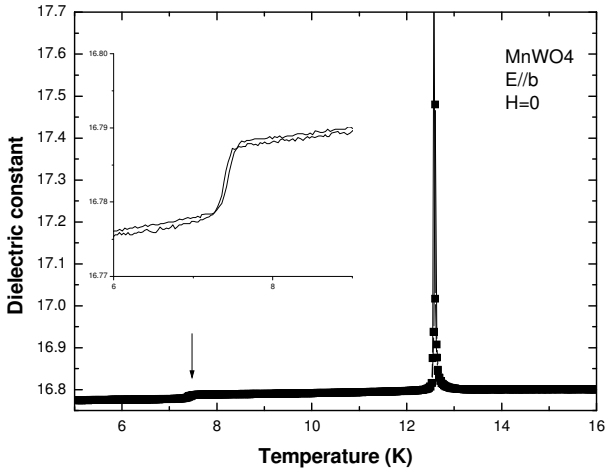

Figure 22: Phase transitions in the dielectric constant

Moreover, the shifts of the dielectric transitions in an applied field show great similarity with the shifts observed in the magnetic transitions. The correlation between the magnetic transitions and the dielectric transitions will be discussed in paragraph 4.5.
To determine the actual polarization in the AFM2 phase, pyroelectric measurements were done on the same samples that were used for the dielectric measurements. The sample was poled with -/+ 100V during the cooling and subsequently the current was measured while increasing the temperature without an applied electric field. By integrating this current over the temperature range the polarization can be found, which is shown in figure 23. The polarization discontinuously sets in around 8 K and from there it gradually drops until the transition around 12.5 K, above which the polarization has disappeared. The measurement was done for several external applied magnetic fields along one of the magnetic axes. Along the x and the y axes the magnetic field induces a large change in the polarization; it suppresses the polarization when applied along the y axis and it stabilizes the polarization when applied along the magnetic x axis.
By changing the sign of the poling voltage the peaks in the current (and with that the polarization) could be reversed completely. Therefore the material is definitely ferroelectric. The measurement was repeated with the electric field applied along the x and the z axes, which resulted in a polarization of 5-8% of the value found in the y direction. It was assumed that this polarization appeared due to misalignment of the crystal and that no true polarization is present on any other axis than the y axis.
The direction of the pyroelectric current, occurring at the transition from the AFM1 to the AFM2 phase, depends on the sign of the voltage that was applied during the cooling of the material. In the measurements shown in figure 23 the voltage as switched off during the measurement. Some other measurements were performed in which the applied voltage during the measurement was the opposite from the voltage applied during poling. It was expected that the polarization would immediately turn towards the direction of the new applied field, and that thus a current would be measured that was opposite to the measurements shown in figure 23.

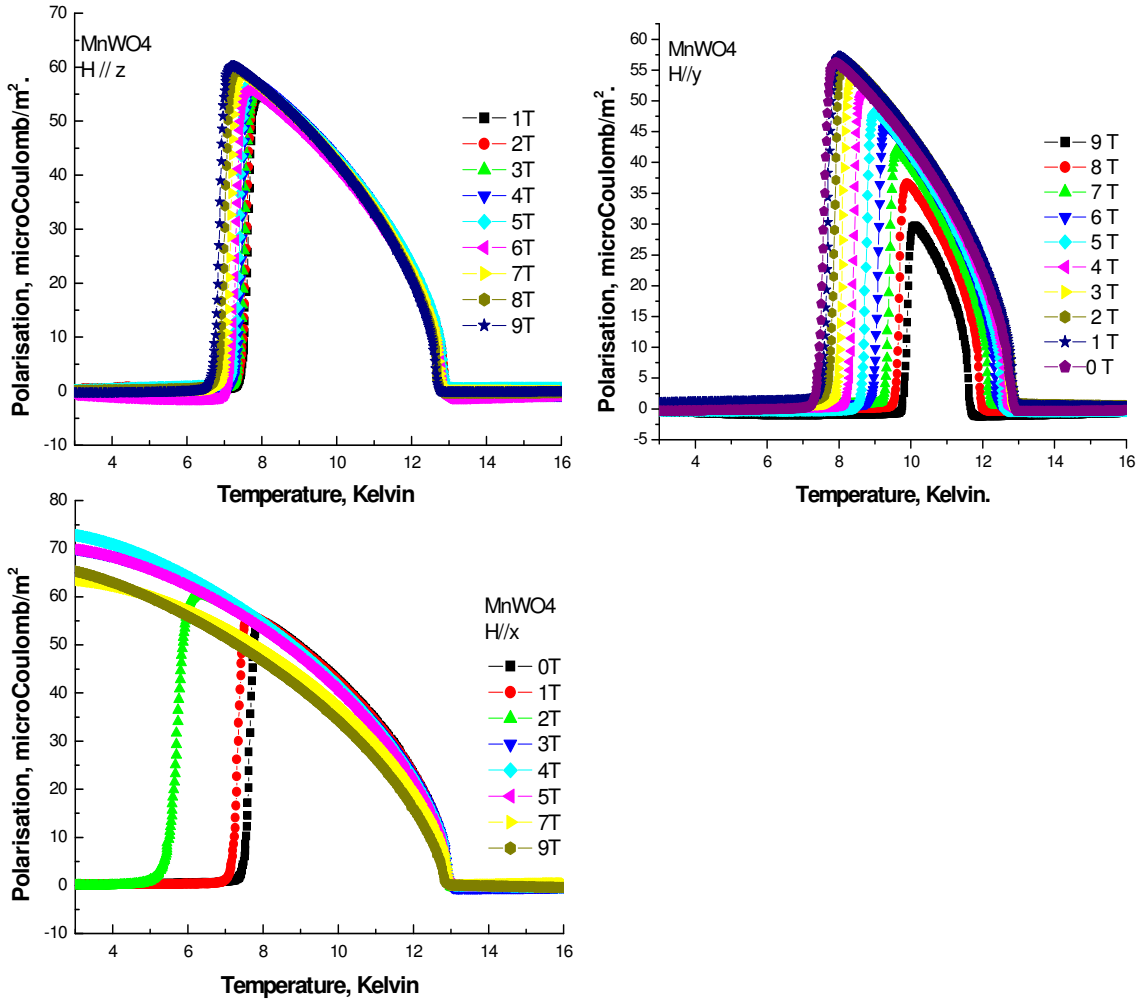

Figure 23: The polarization along the y axis and its magnetic field dependence with the magnetic fields applied along the z (upper left), y (upper right) and x –axis (lower)

However this turn in polarization did not occur until the material was in the AFM2 phase. Accordingly the transition from AFM1 to AFM2 did not depend on the applied voltage during the measurement. It was assumed that this polarization appeared due to a misalignment of the crystal and that no true polarization is present along any other axis than the y axis. Somehow, the AFM1 phase has a memory of the polarization direction present when cooling through the phase transition. This memorized polarization cannot be switched by an opposite electric field.

4.5. Discussion

The phase transitions that were observed in the magnetization experiments on $MnWO_4$ show a magnetic field dependence, which is very similar to the magnetic phase diagrams proposed by Ehrenberg et al.[35]. In addition, the dielectric and pyroelectric transitions demonstrate an identical response towards an applied magnetic field. All transitions are summarized in figure 24.

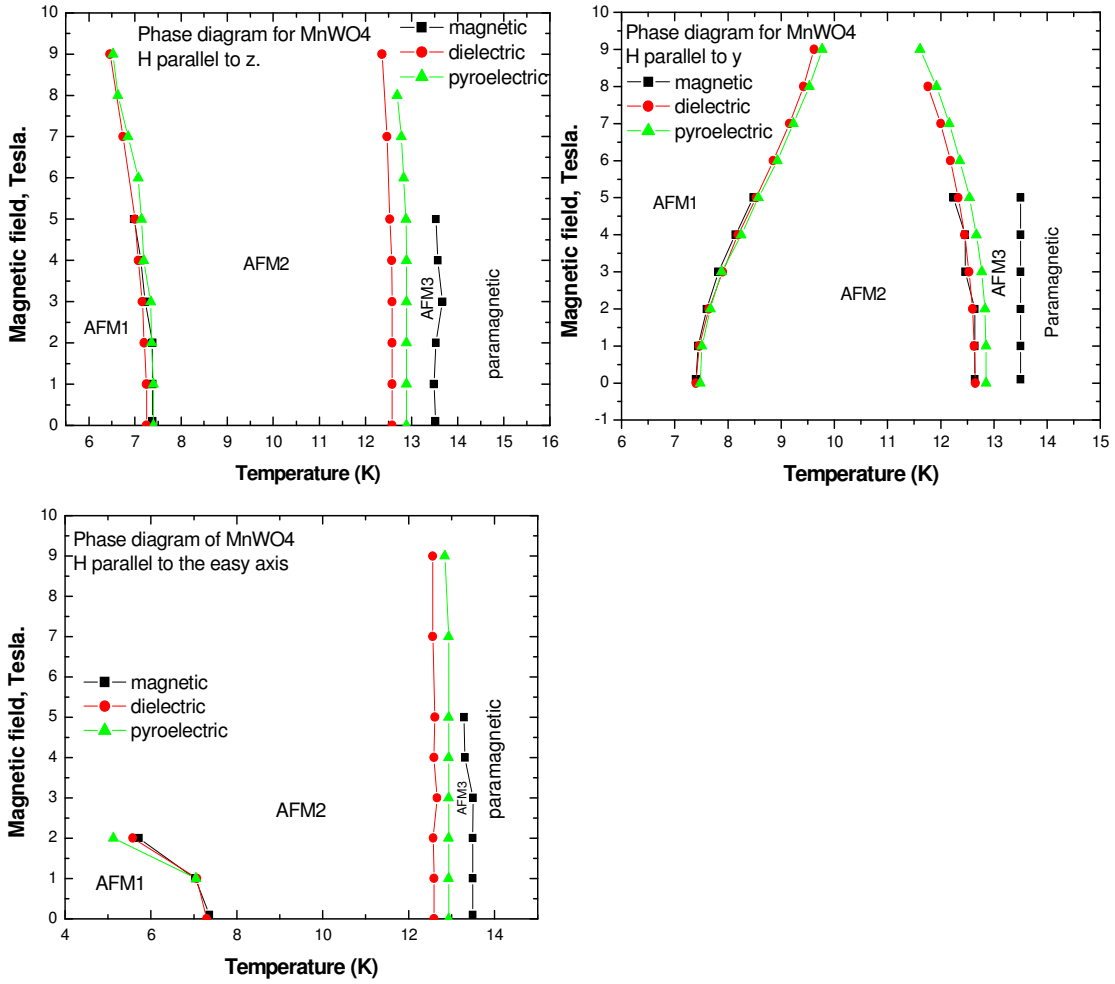

Figure 24: Phase diagram of the magnetic (black), the dielectric (red) and the pyroelectric (green) measurements.

In these graphs the temperature is plotted against the magnetic field for the three different directions of the applied field. The dots represent the conditions at which a transition was observed. The black data are from the magnetic measurements, the red from the dielectric measurements and the green from the pyroelectric measurements.

The similarity between all these transitions is due to the strong coupling between the magnetic and ferroelectric properties in this material. The spiral magnetic phase (AFM2) induces a ferroelectric phase, just as was predicted from the theory. Thus the onset of this helical spin density wave is accompanied by the induction of ferroelectricity that can be observed in dielectric and pyroelectric measurements. The transition from the AFM3 to the paramagnetic phase cannot be observed in this way, because the sine wave does not induce ferroelectricity.

Although the similarity of the different measurements is big, the pyroelectric data seem to correspond to a slightly higher temperature than the other data. This is probably due to the fast change in temperature that was used in these measurements. This high sweeping rate is needed to observe a large current that leads to a sufficient signal to noise ratio.

However, it leads to a less homogeneous temperature distribution and so the transition temperature that was obtained is slightly higher than the actual temperature.
The discontinuous polarization and the shape of the transitions in the dielectric and heat capacity measurements suggest that the transition from the AFM1 to the AFM2 phase is a first order transition. This can explained very well by considering the magnetic wave vectors of both the magnetic structures. The wave vector for the AFM1 phase is (¼, ½, ½) and for the AFM2 the wave vector is (-0.214, ½, 0.457). At the phase transition the wave vector will change abruptly and therefore the transition can only be first order.
The wave vector is the same for both the AFM2 and the AFM3 phase, the only thing that changes being a spin reorientation to go from the helical to the sinusoidal state. Therefore this transition is expected to be second order. The polarization confirms that it is indeed a second order phase transition, as it goes continuously to zero. Furthermore, the peaks in the dielectric constant and the heat capacity that correspond to this transition are more likely to be caused by a second order phase transition.
The dielectric transitions and the pyroelectric current were only observed for the transitions around the AFM2 phase. The spiral magnetic structure led to ferroelectricity while the other magnetic structures did not. Subsequently, the result from the theory summarized in equation 3 (see chapter 2) is correct, and only a spiral magnetic order gives rise to ferroelectricity. Moreover, the polarization was only observed with the electric field applied along the b direction. In $MnWO_4$ the incommensurate wave vector (Q) lies in the ac plane of the crystal. The axis of spin rotation (e_3) also lies in the ac plane, perpendicular to the wave vector. Therefore, according to equation 3, the polarization can only appear along the b axis. Consequently, the observed polarization direction agrees with the prediction made according to the theory that was presented in chapter 1.
The polarization that was observed for this material is approximately 60 $\mu C/m^2$. In general, the polarization that is observed in multiferroics with a magnetically induced polarization is much lower than in ordinary ferroelectrics. The spin density wave seems not to be capable of inducing very large atomic displacement, and thus the polarization is rather low. For example the famous ferroelectric BaTiO3[36] has a polarization of $2.6*10^5$ $\mu C/m^2$, which is about 2 orders of magnitude higher than the highest polarization observed for materials with ferroelectricity due to magnetic order.
An overview of most materials that show ferroelectricity due to magnetic order is given in table 6. The polarizations for these materials range from 4 to 3000 $\mu C/m^2$. The value of 60 $\mu C/m^2$, found for the polarization in $MnWO_4$, fits within this range of polarizations. However, it is hard to explain the differences in polarization within this subclass of multiferroics, because it is still unclear how the polarization depends on the characteristics of the magnetic spiral. Probably the crystallographic and the electronic properties, as well as the details of the magnetic order, influence the magnitude of the polarization in these materials.
Although the ferroelectricity only appears in the AFM2 phase, the experiments showed that the AFM1 phase remembers the polarization direction. There is a, probably correlation between these two magnetic structures, which preserves the polarization direction even when the ferroelectricity has gone. A phase coexistence of the AFM1 and the AFM2 could also account for the memorization of the polarization direction. However, such phase coexistence is unlikely to show the obtained indifference towards

an opposing electric field. More (inelastic) neutron scattering experiments could provide insight into these question.

Table 6: An overview of all materials that show ferroelectricity due to magnetic ordering.

Material	Wave vector	Crystal symmetry	Temp. Range (K)	P $\mu C/m^2$	Notes
$Ni_3V_2O_8$ [37, 5, 38]	(0.28, 0, 0)	Cmca orthorhombic	3.9-6.3	100	
$GdMnO_3$ [4]	(0, 0.195, 0)	Pbnm orthorhombic	< 21	3000	In magnetic field only.
$TbMnO_3$ [4]	(0, 0.28, 1)	Pbnm orthorhombic	< 28	600	
$DyMnO_3$ [4]	(0, 0.385, 0)	Pbnm orthorhombic	< 18	1500	
$Ba_{0.5}Sr_{1.5}Zn_2Fe_{12}O_{22}$ [39]	(0, 0 3d) 0<d<1/2	R-3m rhombohedral	< ≈ 400	150	In magnetic field only.
$TbMn_2O_5$ [40, 41]	(0.47, 0, 0.28)	Pbam orthorhombic	< 28	4	
$GdMn_2O_5$ [40]	?	Pbam orthorhombic	< 25	10	

4.6. Conclusion

The use of the floating zone technique to grow $MnWO_4$ crystals was very successful. This new way of synthesizing $MnWO_4$ crystals resulted in larger crystals than obtained with the flux method that was used in earlier studies of this material. Moreover, x-ray diffraction experiments showed that the floating zone crystals were very pure and without any pollution whereas the flux grown crystals contained a pollution of Mn_2O_3 of a few mol percent. Determination of the heat capacity showed that this pollution significantly changed the phase transitions in the material. Therefore the improved crystal quality has resulted in more reliable measurements, which have revealed a clearer view of the physical properties of $MnWO_4$.

In the $MnWO_4$ crystal the magnetic interactions are frustrated, such that three different magnetic structures are present below 13.5 Kelvin. Between 8 and 12.5 Kelvin a structure is present that consists of a helical incommensurate spin density wave. Recent theories on magnetically induced ferroelectricity predict that a spiral magnetic ordering will result in an electrical polarization. Dielectric and pyroelectric measurements show that the onset of the magnetic spiral structure in $MnWO_4$ is accompanied by the induction of a polarization perpendicular to the spin rotation axis and the wave vector.

The available theories on magnetically induced ferroelectricity are successful in predicting which magnetic structures give rise to polarization and in which direction. But there is no description of the magnitude of the polarization that is able to explain the differences in polarization between $MnWO_4$ and the other magnetically induced ferroelectrics.

Another subject that needs improvement is the understanding of the magnetic frustration in $MnWO_4$. (Inelastic) Neutron scattering experiments could shed some light on the

complex magnetic interactions that lead to frustration in this material. It would be very interesting to obtain the correlation between the AFM1 and the AFM2 phase, and to determine how the AFM1 can remember the polarization direction in the AFM2 phase.
$MnWO_4$ is a completely new multiferroics material. It is different in structure to other systems that show this type of magnetically induced ferroelectricity. Nevertheless, it shows the same strong coupling between magnetic and ferroelectric order. As the number of materials that show these properties is small, the discovery of magnetically induced ferroelectricity in $MnWO_4$ will play an important role in the further development of the theory of the interactions in this type of materials. Accordingly, although the polarization and the temperature of the multiferroic phase in $MnWO_4$ might not be ideal for implementation in industry, the discovery will have an important contribution to the understanding and further development of multiferroics.

Chapter 5: Summary and Prospects

Summarizing the research mentioned in this report, the x-ray diffraction and heat capacity measurements on FeS show a clear transition at 400 K, the temperature at which the ferroelectric phase transition was reported by van den Berg et al.[8] At this alpha transition an abrupt change in the lattice parameters was observed. Moreover an anomaly could be observed in the electrical resistivity. The magnetization at high temperatures could not be measured due to failing equipment, but the magnetization at lower temperature showed a transition around 160K that has never been reported before. The conductivity in the material was too high to pole the sample and thus no pyroelectric measurements could be performed. Therefore the question of whether FeS is a possible candidate for ferroelectricity at room temperature remains unanswered.

The $MnWO_4$ results are useful in developing the theory of ferroelectricity in spiral magnetic structures. For the first time the floating zone technique was used to grow crystals of $MnWO_4$. This new way of synthesizing $MnWO_4$ crystals resulted in larger crystals than obtained with the flux method that was used in earlier studies. Moreover, x-ray diffraction experiments showed that the floating zone crystals were very pure and without any pollution whereas the flux grown crystals contained a pollution of Mn_2O_3 of a few mol percent. The improved crystal quality has resulted in more reliable measurements, which have revealed a clearer view of the physical properties of $MnWO_4$. In the $MnWO_4$ crystal the magnetic interactions are frustrated, such that three different magnetic structures are present below 13.5 K. Between 8 and 12.5 K the magnetic structure consists of a helical incommensurate spin density wave. The recent theories[6] on ferroelectricity induced by magnetic ordering predicted that a spiral magnetic ordering will result in an electrical polarization. Dielectric and pyroelectric measurements show that the onset of the magnetic spiral structure in $MnWO_4$ is accompanied by the introduction of a polarization perpendicular to the spin rotation axis and the wave vector. These measurements showed that the spiral magnetic phase of $MnWO_4$ is indeed multiferroic. As the number of materials that show these properties is small, the discovery of ferroelectricity due to magnetic ordering in $MnWO_4$ will play an important role in the further development of the theory of the interactions in this type of materials.

This research project was performed out of scientific interest and curiosity about the interplay between ferroelectric and magnetic order in materials. As mentioned in the introduction however, these multiferroics might be interesting for implementation in to data storage media used by the computer industry. The ideal multiferroic for this purpose would be a material that is strongly ferroelectric and ferromagnetic. Moreover it should posses a strong magnetoelectric effect and all these features should be present at room temperature. The recent discovery of materials that have a ferroelectricity induced by magnetic ordering is very promising, because it is the only group of multiferroics in which the coupling between magnetic and electric properties is significant enough to be used in devices.

A very promising development is the discovery of multiferroicity in the hexaferrite $Ba_{0.5}Sr_{1.5}Zn_2Fe_{12}O_{22}$ [39]. In this material the spiral magnetic phase and its polarization exist up to room temperature. The material is antiferromagnetic and has a ferroelectric polarization of $150\mu C/m^2$. The main problem with this material is the electrical

conductivity at room temperature, which is so high that poling becomes difficult. However, as this class of materials is very versatile, it is expected that both the magnetic moment and the conductivity can easily be optimized by tuning the composition. Therefore, the hexaferrites might be a good candidate for implementation in industry.
Another nice development was presented by Yamasaki et al.[42] who recently found that $CoCr_2O_4$ shows multiferroicity. Instead of the spiral structure this material has a conical magnetic structure, which results in a ferrimagnetic order with a net magnetic moment. The direction of the rotation in the magnetic spiral structure determines the orientation of the polarization in spiral magnets. In this conical structure the magnetic moment is also determined by the rotation direction of the spins and thus the polarization can be switched by switching the direction of the magnetic moment using an external magnetic field. Thus, by applying a magnetic field one can completely switch the polarization.
In general, the biggest problems for multiferroics will be the electrical conductivity at room temperature and the relatively low electric polarization. Ferromagnets are often not very good insulators. For multiferroics this high conductivity is a severe problem because the ferroelectricity is killed when the polarization is screened by mobile charges. Moreover the high conductivity makes poling of the polarization direction impossible because the application of high voltages will induce such high currents that the material will burn. Therefore it is essential for a multiferroic to show a high resistivity.
The other main problem is the size of the electric polarization for the materials in which the magnetic structure causes the ferroelectricity. This polarization is much smaller than in regular ferroelectrics and it seems that this will remain rather low during the development of this class of materials as it is an intrinsic property of ferroelectricity induced by magnetic order.

Acknowledgement

I would like to thank Thom Palstra for his supervision during the whole period of research that led to this master thesis. I thank Graeme Blake for his supervision during the research on iron sulfide. Besides I would like to thank Art Ramirez and Tsuyoshi Kimura for their supervision during the research on $MnWO_4$. Moreover I need to thank Maxim Mostovoy for his comments, Auke Meetsma for his help with the x-ray diffraction measurements and Jacob Baas, Jan de Boer and Jan Spoelstra for their technical assistance. I thank Christian Kloc for the use of his coffee machine and Theo Siegrist for the nice discussions. Finally I would like to thank Gernot Krabbes and Gerrit Wiegers for their advise on the synthesis on the FeS crystals.

References

[1]: D.I Khomskii, Journal of Magnetism and Magnetic Materials, in press
[2]: T. Kimura, T. Goto, H. Shintani, K. Ishizaka, and T. Arima and Y. Tokura, Nature **426**, 55 (2003).
[3]: N. Hur, S. Park, P.A. Sharma, J.S. Ahn, S. Guha and S-W. Cheong, Nature **429**,392 (2004)
[4]: T. Kimura, G.Lawes, T. Goto, Y. Tokura, A.P. Ramirez, Phys. Rev. B **71**, 224425 (2005).
[5]: G. Lawes, A.B. Harris, T. Kimura, N. Rogado, R.J. Cava, A. Aharony, O. Entin-Wohlman, Y. Yildrim, M. Kenzelmann, C. Broholm and A.P. Ramirez, Phys. Rev. Lett. **95**, 087205 (2005).
[6]: M. Mostovoy, Phys. Rev. Lett. **96**, 067601 (2006)
[7]: G.A. Smolenskii and I.E. Chupis, Sov. Phys. Usp.**25**, 475 (1982).
[8]: C.B.van den Berg, J.E. van Delden, J. Bouman, Phys. Stat. Sol. **36**, K89 (1969)
[9]: H. Ehrenberg, H. Weitzel, H. Fuess and B. Hennion, J. of Phys. Cond. Matt. **11**, 2649(1999).
[10]: M. Fiebig, J. Phys. D: Appl. Phys. **38**, R123 (2005).
[11]: N.A. Hill, J. Phys. Chem. B **104**, 6694 (2000).
[12]: B.B. van Aken, A.Meetsma and T.T.M. Palstra, Acta Cryst. **E57**, i87(2001).
[13]: M. Eibschütz and H.J. Guggenheim, Solid State Comm. **6**, 737 (1968)
[14]: I.A. Sergienko and E. Dagotto, Phys. Rev. B **73**, 094434 (2006).
[15]: T. Moriya, Phys. Rev. **120**, 91 (1960).
[16]: I. Dzyaloshinskii, J. Phys. Chem. Solids **4**, 241 (1958).
[17]: F. Li, H.F. Franzen, Journal of Alloys and Compounds **238**, 73 (1996).
[18]: C.B. van den Berg, Ferroelectrics **4**, 117-120 (1972).
[19]: G. Collin, M.F. Gardette and R. Comes. J. Phys. Chem. Solids **48**, 791(1987).
[20]: H.E. King and C.T. Prewitt, Acta. Cryst. B **38**, 1877 (1982)
[21]: J.V. Cathcart, R.E. Druschel, L. Manley and G.F. Petersen, Journal of Crystal Growth **62**, 299 (1982).
[22]: G. Krabbes, H. Oppermann and E. Wolf, Zeitschrift fur Anorganische und Allgemeine Chemie **423**, 212 (1976).
[23]: A.C. Larson and R.B. Von Dreele, General Structure Analysis System (GSAS), Los Alamos National Laboratory Report LAUR 86-748 (2004).
[24]: W.C.Hamilton, Acta Cryst. **18**, 502 (1965)
[25]: R. Perthel, Annalen der Physik **7** (folge) **5** (band), 273 (1960).
[26]: J. M. D. Coey, H. Roux-Buisson and R. Brusetti, Journal de physique, Colloque C4-1 (1976).
[27]: G. Lautenslager, H. Weitzel, T. Vogt, R. Hock, A. Böhm, M. Bonnet, H. Fuess, Physical Review B **48**, 6087 (1993).
[28]: H. Ehrenberg, H. Weitzel, H. Fuess and B. Hennion, Journal of Physics Condensed Matter **11**, 2649(1999).
[29]: J. Goodenough, Physical Review **6**, 1442 (1960).
[30]: J. Kanamori, J. Phys. Chem. Solids (Pergamon press) **10**, 87 (1959).
[31]: H. Dachs, Solid State Communications **7**, 1015 (1969).

[32]: H. Weitzel and H. Langhof, Journal of Magnetism and Magnetic Materials **4**, 265 (1977).
[33]: B.M. Wanklyn, Journal of material science **7**, 813 (1972).
[34]: C. Kittel, " introduction to solid state physics", John Wiley and Sons, seventh edition (1996), page 464.
[35]: H. Ehrenberg, H Weitzel, C. Heid, H Fuess, G. Wltschek, T. Kroener, J. van Toll, M. Bonnet, Journal of Physics Condensed Matter **9**, 3189(1997).
[36]: F. Jona and G. Shirane, "ferroelectric crystals", Dover Publications, New York (1962).
[37]: N. Rogado, G. Lawes, D.A. Huse, A.P. Ramirez, R.J. Cava, Solid State Communications **124**, 229 (2002).
[38]: G. Lawes, M. Kenzelmann, K.H. Kim, G.A. Jorge, R.J. Cava, A. Aharony, O. Entin-Wohlman, A.B. Harris, T. Yildrim, Q.Z. Huang, S. Park, C. Broholm and A.P. Ramirez, Physical Review Letters **93**, 247201 (2004).
[39]: T. Kimura, G. Lawes, A.P. Ramirez, Physical Review Letters 94, 137201 (2005).
[40]: A. Inomata and K. Kohn, Journal of Physics Condensed Matter 8, 2673 (1996).
[41]: S. Kobayashi, H. Kimura, Y. Noda and K. Kohn, Journal of the Physical Society of Japan 74, 468 (2005).
[42]: Y. Yamasaki, S. Miyasaka, Y. Kaneko, J.-P. He, T. Arima and Y. Tokura, Phys. Rev. Lett. **96**, 207204 (2006)